PNAS

Main Manuscript for

Covalent anti-HIV compound that induces HIV-1 capsid multimerization and degradation decomposes the viral core

Tomofumi Nakamura[a,b*], Nobutoki Takamune[c], Mayu Okumura[a], Jun-ichiro Yasunaga[a], Masaharu Sugiura[d], and Masayuki Amano[a,e*].

[a] Department of Hematology, Rheumatology, and Infectious Diseases, Graduate School of Medical Sciences, Faculty of Life Sciences, Kumamoto University, Kumamoto 860-8556, Japan

[b] Department of Laboratory Medicine, Kumamoto University Hospital, Kumamoto 860-8556, Japan

[c] Headquarters for Research and Development Strategy, Kumamoto University Kumamoto 860-0862, Japan

[d] Faculty of Pharmaceutical Sciences, Sojo University, Kumamoto 860-0082, Japan

[e] Kumamoto Daiichi Hospital, Kumamoto 862-0965, Japan

*Tomofumi Nakamura, **Email**: tomona@kumamoto-u.ac.jp

*Masayuki Amano, **Email**: mamano@kumamoto-u.ac.jp

Author Contributions: Author Contributions: T. N. and M.A. designed research; T.N., N.T., M.O., M. S., and M.A. performed research; M.S. contributed new compounds; T.N., N.T., M.O., M.S., and M.A. analyzed data; N.T., M.S., and J.Y. edited the paper; J.Y. and M.A. supervised personnel and the study; T.N. and M.A. wrote the paper.

The authors declare no competing interest.

Classification: Biological Sciences, Pharmacology

Keywords: HIV, HIV capsid inhibitor, covalent inhibitor, HIV capsid multimerization and degradation

This PDF file includes:

Main Text
Figures 1 to 6
Tables 1 to 3

Abstract

Drugs that covalently bind to their target molecules form strong and irreversible interactions with each other. Covalent inhibitors have recently attracted attention because of their enhanced structural selectivity within the target cavity, which results in prolonged interactions, even at low doses. Here, we report that ACAi-001 is a human immunodeficiency virus (HIV)-1 capsid (CA)-targeting compound with covalent binding to CA, estimating long-lasting effects for HIV inhibition. Using a library of millions of compounds, ACAi-001 was identified through *in silico* screening. This compound is designed to target the hydrophobic cavity in the N-terminal domain of CA and, in a cell-based assay, was found to inhibit HIV-1 replication. ACAi-001 covalently bound to CA and induced aberrant CA multimerization and degradation, as assessed by western blotting, size-exclusion chromatography, thermal stability assay, enzyme-linked immunosorbent assay, and liquid chromatography-mass spectrometry. ACAi-001, which has two putative covalent interactions in its chemical structure, binds directly to serine 16 in the N-terminal domain-targeting cavity and to cysteine 198 or 218 in the C-terminal domain of CA. This unique binding profile of ACAi-001 to CA induces multiple CA dysfunctions such as CA multimerization and degradation, resulting in disruption of the HIV core, thereby inhibiting HIV-1 infection and replication. ACAi-001, which covalently binds to and degrades CA in an unique manner, may reveal new aspects of HIV core assembly and disassembly and is a promising candidate as a next-generation anti-HIV-1 CA inhibitor.

Significance Statement

Lenacapavir (LEN) is a first-in-class CA inhibitor used clinically to inhibit HIV-1 replication. LEN is a long-acting capsid inhibitor with a convenient dosing regimen and is effective for both treating multidrug-resistant HIV and as pre-exposure prophylaxis. ACAi-001 targets specific CA cavities and covalently binds to CA in a distinct manner from LEN. ACAi-001 forms two covalent interactions with CA, leading to CA multimerization and degradation to cause multiple CA dysfunctions. Therefore, more potent derivatives of ACAi-001 with covalent interactions may serve as long-acting capsid inhibitors. ACAi-001 shows potential as a next-generation HIV-1 capsid inhibitor against HIV-1 infection and can be used to reveal details on HIV core assembly and disassembly in the HIV-1 life cycle.

Introduction

During human immunodeficiency virus type 1 (HIV-1) replication, immature virions bud from infected cells and begin to mature through the proteolytic processing of Gag and Gag-pol precursor proteins. HIV-1 protease (PR) cleaves the Gag precursor Pr55 into three distinct structural proteins [matrix (MA, p17), capsid (CA, p24), and nucleocapsid (NC)] and three peptides [spacer peptides 2 and 1 (p2 and p1, respectively), and p6] (1, 2). CA, cleaved from the Gag polyprotein assembly, forms hexamers and pentamers on a mature cone-shaped CA (HIV core) (3, 4). We previously reported that amino acid (AA) insertions at specific positions in HIV-1 CA cause significant CA degradation and that HIV-1 variants carrying such AA insertions significantly impaired infectivity and replicability. We hypothesized that the observed CA degradation was due to conformational/structural incompatibility caused by AA insertion at a specific site on CA (5). Small molecules can interact with target proteins through various binding modes; recently, potent interactions such as covalent binding have attracted attention (6). Covalent drugs react covalently with their target proteins and irreversibly inhibit their biological functions. Drugs such as aspirin and penicillin are well-known examples of covalent drugs (7) that were not intentionally designed as covalent drugs. Covalent drugs exert strong and sustained effects by irreversibly binding to their target proteins. In addition, they can react with specific amino acid residues in proteins to selectively inhibit protein families or subtypes, even though non-covalent small-molecule ligands interact poorly with them (8). In contrast, covalent drugs may cause side effects by reacting nonspecifically with off-target proteins or other biological components (9). In the last decade, new types of covalent drugs have been developed that are precisely and molecularly designed to react with target proteins, known as targeted covalent inhibitors, for anticancer therapy (7, 10).

From the above, we predicted that a compound tightly bound to a specific degradation-inducing region(s) of CA can lead to CA degradation and suppress viral replicability. In the present study, we searched for compounds capable of binding to such hydrophobic regions on the surface of CA using *in silico* docking simulation by processing a library containing millions of compounds, and evaluated the anti-HIV-1 activity of the compounds with better docking scores. We also investigated the effect of newly selected anti-HIV-1 compounds on CA proteins expressed in *Escherichia coli*, 293T, or COS7 cells, and viral lysates/suspensions of HIV-1_{NL4-3}. The design of covalent compound drugs, such as ACAi-001, which induces CA multimerization and degradation, may uncover the mechanism of action for HIV core formation. Moreover, ACAi-001 may reveal the role of the cavity of CA that have not been previously targeted during HIV-1 replication.

Here, we highlight that ACAi-001 utilizes unique mechanisms of action how to interfere with HIV-1 life cycle.

Results

ACAi-001 binding profile to the new target hydrophobic cavity on CA.

As we previously reported, an AA insertion between Arg18-Thr19 near the target cavity of HIV-1 CA causes conformational and structural incompatibility of CA, leading to CA degradation (5). We hypothesized that a small compound that binds tightly or covalently to the target cavity could induce CA degradation. The hydrophobic cavity at the N-terminal domain of CA (CA-NTD) was of a suitable size (252.8 $Å^3$) based on crystallographic data of the CA monomer (PDB ID: 3H47) (Fig. 1*A*) (11) and had sufficient space for certain small compounds to potentially fit snugly in the cavity (Fig. S1*A*). This target cavity of the CA-NTD in the center of the CA hexamer may also affect CA hexamer formation (Fig. 1*B*). We then extracted 6,842,684 compounds from a commercially available library of 8,555,483 compounds that were expected to exhibit good *in vivo* pharmacokinetics based on the number of H-bond donors and acceptors, molecular weight, calculated log P, and number of rotatable bonds, which are related to the absorption distribution metabolism excretion of compounds that can be taken orally (Table 1). Next, the simulated binding scores of each compound to the target cavity were calculated using a virtual docking simulation algorithm, and compounds with good binding scores were further evaluated using cell-based HIV-1 drug susceptibility assays (Fig. S1*B*). To date, we have identified more than 40

active compounds against HIV-1_{LAI} (12) using a 3-(4,5-dimethylthiazol-2-yl)-2,5-diphenyltetrazolium bromide (MTT) screening assay; these compounds showed no or low cytotoxicity against MT-2 and MT-4 cells which are lymphoblastic leukemia-derived T cells. One of these compounds, ACAi-028 binds noncovalently to the target cavity (13) and exerts anti-HIV-1 activity. The chemical structure of ACAi-001 and putative binding structures of ACAi-001 to CA are shown in Fig. 1*C*. In this study, ACAi-001, which exhibited potent anti-HIV-1 activity (Table 2) and lower cytotoxicity (Table 3), was investigated to understand the details of its anti-HIV-1 activity.

ACAi-001 binding covalently to CA induces CA multimerization and degradation.
To investigate the direct binding of ACAi-001 to CA, we purified CA proteins expressed in *E. coli* (Fig. S2*A*). Evaluation using liquid chromatography-mass spectrometry (LC-MS) showed that 1, 2, and 3 ACAi-001 molecules bound to the CA monomer under native conditions (Fig. S2*B*). One and two ACAi-001 molecules were found to interact with the CA monomer under denaturing conditions involving treatment with acetonitrile and trifluoroacetic acid (Fig. 2*A*), suggesting that ACAi-001 directly and covalently bound to CA proteins similar to ebselen (Eb), a covalent capsid inhibitor (14). The actual molecular weight (MW) of the ACAi-001 plus CA monomer detected using LC-MS was five units smaller compared to the calculated MW of the ACAi-001 plus CA monomer, suggesting that the MW was reduced by covalent binding with structural changes between ACAi-001 and CA (Fig. S2*C*). In addition, CA proteins were incubated with ACAi-001, ACAi-028, the HIV-1 integrase (IN) inhibitor raltegravir (RAL) (15), and the capsid inhibitor PF74 (16), which is a lead compound of lenacapavir (17), for 72 h in reaction buffer. The results showed that large amounts of CA multimers and degradation products induced by ACAi-001 were detected by western blotting (WB) with an anti-CA antibody (Fig. 2*B*) under denaturing conditions compared to the effects of ACAi-028, RAL, and PF74. CA multimerization began to occur after 3 h in the presence of 100 μM of ACAi-001, whereas CA degradation products appeared after 12 h (Fig. S2*D*). These CA abnormal products were observed in more than 20 μM of ACAi-001 (Fig. S2*E*). When the samples were treated at different temperatures, CA multimerization and degradation were induced at higher temperatures (Fig. S2*F*). Moreover, many CA proteins of unidentifiable sizes, including CA monomers, appeared as broad peaks 24 h after ACAi-001 treatment using size-exclusion chromatography (SEC) (Fig. 2*C,* Fig. S2*G*). To determine whether the covalent interactions of ACAi-001 were non-specific, we confirmed the effect of ACAi-001 on bovine serum albumin (BSA). When BSA was analyzed using WB with a BSA antibody after treatment with dimethyl sulfoxide (DMSO) or ACAi-001 for 72 h, no abnormal BSA multimerization or degradation was observed in ACAi-001-treated samples, as observed for CA proteins (Fig S2*H*). Next, we examined the profiles of CA multimerization (18) and thermal stability (19) after addition of ACAi-001 (Fig. 2*D* and *E*, Fig. S2*I* and *J*). Interestingly, the experimental CA multimerization induced by a high sodium concentration was impaired after treatment by more than 20 μM ACAi-001, suggesting that abnormal CA multimerization and degradation interfere with such experimental CA multimerization, unlike the effects of RAL. The thermal stability of CA was severely decreased by -8.4°C and -12.4°C at 20 and 200 μM ACAi-001, respectively, after 72 h of treatment (Fig. 2*E*), suggesting that ACAi-001-induced aberrant CA multimerization and degradation led to the loss of normal physiological multimerization and thermal stability of CA.

CA multimerization and degradation induced by ACAi-001 are readily detected by WB and p24 enzyme-linked immunosorbent assay.
To detect CA multimerization and degradation induced by the selected compounds, the states of CA were evaluated and measured as the CA immunogenicity using WB and an automated enzyme-linked immunosorbent assay (ELISA) device (Lumipluse G1200). We constructed plasmids expressing wild-type HIV-1_{NL4-3} CA (CA^{WT}). Cell lysates containing CA^{WT} were incubated with ACAi-001 for different times (0, 24, 48, and 72 h) at 37°C and then evaluated for CA immunogenicity. Interestingly, the immunogenicity of CA monomers treated with ACAi-001 decreased significantly in a time-dependent manner and was less than 20% within 72 h of

incubation compared to that in the DMSO control (Fig. 3*A* and Fig. S3*A*), suggesting that ACAi-001 induces aberrant multimerization and degradation of CA derived from the cell lysates. In contrast, the amount of CA^{WT} was not significantly reduced when cell lysates containing CA^{WT} incubated with DMSO and PF74 were used as negative controls (Fig. 3*B*). Next, we examined the profiles of CA treated with ACAi-001 using lysates of infectious HIV-1_{NL4-3} (HIV^{WT}) by ELISA and WB analyses. Figure 3*C* and *D* show that ACAi-001 also significantly reduced CA immunogenicity in the lysate containing HIV^{WT} viral particles, CA immunogenicity in ELISA was reduced by less than 20% within 24 h of incubation in the ACAi-001-treated sample, and only a small reduction was observed in DMSO. We evaluated the effects of the first-in-class HIV-1 CA maturation inhibitors bevirimat (20) and PF74 on CA. As shown in Fig. 3*D*, bevirimat and PF74 did not reduce CA immunogenicity, suggesting that ACAi-001 exerts a different mechanism(s) of interaction with CA than that of other HIV-1 CA inhibitors. Figure 3*E* shows that the CA immunogenicity induced by ACAi-001 was reduced in a dose-dependent manner. Additionally, ACAi-001 reduced HIV-2_{ROD} (37) CA immunogenicity, even in the lysates of HIV-2_{ROD}-infected MT-2 cells (Fig. 3*F*). Furthermore, ACAi-001 induced CA degradation as assessed using cell lysates from peripheral blood mononuclear cells infected with four different subtypes of clinically isolated HIV-1 strains (Fig. S3*B*). These results indicate that ACAi-001 can induce multimerization and degradation of recombinant CA protein expressed in the cell lysates and CA in HIV^{WT} particles, which were readily detected using WB and p24 ELISA.

Putative covalent bond-forming structures in ACAi-001.

ACAi-001 has two potential moieties, hydroquinone and hydrazide, that can react covalently with CA proteins (Fig. 4*A*) (21). The hydroquinone structure of ACAi-001 can be converted to *p*-benzoquinone via oxidation, which likely produces one covalent bond with a specific AA residue such as cysteine, including a thiol group in the CA protein. The hydrazide of ACAi-001 initiates a nucleophilic substitution reaction to form a second covalent bond with another CA protein. It is expected that an ACAi-001 can covalently bond to two CA proteins, forming a hinge (Fig. 4*A*), which may induce aberrant CA multimerization. To examine these reactions between CA proteins and ACAi-001, we added the reducing agent β-mercaptoethanol (βME) to the reaction buffer to prevent oxidation of the hydroquinone. As shown in Fig. 4*B* and Fig. S4, aberrant CA multimerization was found in the normal reaction buffer after treatment with more than 20 μM of ACAi-001 for 24 h, whereas such aberrant CA multimerization was completely inhibited by addition of 10 mM βME. In addition, ANS-1028 and ANS-1050 were converted from the hydroquinone structure of ACAi-001 to a meta- or ortho-phenol structure, excluding one hydroxyl group from the benzene ring of ACAi-001 (Fig. 4*C*). As expected, ANS-1028 and ANS-1050 did not cause CA multimerization and degradation, nor did PF74 and Eb (Fig. 4*C* and Table S2). These results indicate that the hydroquinone structure of ACAi-001 is critical for the formation of covalent bonds in CA, which induce aberrant CA multimerization and degradation.

ACAi-001 binds to a serine residue in the target cavity of CA-NTD and cysteine residues in CA-CTD.

In silico docking simulation targeted the hydrophobic cavity on the N-terminal surface of CA (Fig. 1*A*). To investigate how ACAi-001 interacts with specific AAs and induces CA multimerization and degradation, we constructed a plasmid expressing CA truncated at the N-terminal AAs (CA-$NTD^{\Delta 1-100}$). As shown in Fig. S5*A*, the cell lysates of COS-7 cells expressing CA-$NTD^{\Delta 1-100}$ incubated for 72 h with ACAi-001 showed no significant structural changes similar to those with DMSO, suggesting that ACAi-001 requires full-length CA to induce CA multimerization and degradation.

ACAi-001, carrying electrophilic reactive groups, hydroquinone and hydrazide, can covalently and irreversibly bind to nucleophilic AA residues in the target CA protein. We predicted that ACAi-001 has the potential to form covalent bonds with some cysteine and serine residues of CA (9, 21). To distinguish the putative ACAi-001 binding cavities, we named the target cavity in the NTD of CA, ACAi-pocket, and other cavity carrying two cysteines in the C-terminal domain of CA, as the Cys-pocket, as shown in Fig. 5*A*. To confirm whether ACAi-001 interacts with the AA residues in these

target cavities (Fig. 5*A*), we produced CA variants carrying S16E (CA^{S16E}) in the ACAi-pocket, C198A/C218A ($CA^{C198A/C218A}$) in the Cys-pocket, or S16E/C198A/C218A ($CA^{S16E/C198A/C218A}$) in both pockets, which may alter the binding ability of ACAi-001 to CA. Sequence analysis of 12,261 HIV-1 sequences (all subtypes; Los Alamos HIV Sequence Database) using WebLogo 3 showed high conservation of key residues: S16 within the ACAi-pocket and C198 and C218 within the Cys-pocket. SEC analysis showed aberrant CA^{WT} multimerization with two broad peaks and CA^{WT} degradation on a gentle slope after treatment with ACAi-001 for 24 h, compared with those in the DMSO control (Fig. 5*B*). Although the peaks of CA^{S16E} and $CA^{C198A/C218A}$ multimerization and degradation induced by ACAi-001 treatment decreased, the peaks of $CA^{S16E/C198A/C218A}$ induced by ACAi-001 were similar to those following DMSO treatment (Fig. 5*B*). In line with the SEC results, CA^{WT} multimerization was induced in a dose-dependent manner by ACAi-001 (5, 10, and 20 μM) under denaturing conditions according to WB, whereas CA^{S16E} multimerization and $CA^{C198A/C218A}$ multimerization were slightly and strongly decreased after treatment with ACAi-001 for 24 h. The multimerization of $CA^{S16E/C198A/C218A}$ carrying these three mutations induced by ACAi-001 almost disappeared, as shown in Fig. 5*C*. In addition, binding of ACAi-001 to $CA^{S16E/C198A/C218A}$ significantly decreased under LC-MS denaturing conditions. The binding peaks of the calculated MW of $CA^{S16E/C198A/C218A}$ plus ACAi-001 disappeared, except for a negligible peak of one ACAi-001 binding event (Fig. 5*D*, Fig. S5*B* and *C*). These results suggest that ACAi-001 covalently interacts with both Ser16 residue in the ACAi-pocket and Cys198/Cys218 residues in the Cys pocket.

Effect of ACAi-001 on the early- and late-stage of HIV-1 life cycles.

We investigated the time point at which the anti-HIV-1 activity of ACAi-001, which induces CA multimerization and degradation, is exerted during the HIV-1 life cycle. To examine early-stage inhibition by ACAi-001, we performed TZM-bl cell and colorimetric reverse transcriptase (RT) activity assays. ACAi-001 did not significantly inhibit the early-stage of pseudo-type VSV-G HIV-1_{dENV}; similar results were observed when using a protease inhibitor, darunavir (DRV) (22), in contrast to the effects of an RT inhibitor, zidovudine (23) and RAL, when the drugs and VSV-G HIV-1_{dENV} were simultaneously used to treat TZM-bl cells (Fig. S6*A*). We also examined whether ACAi-001 prevents HIV-1 RT activity using a colorimetric RT assay. ACAi-001, DMSO, and PF74 did not significantly impact HIV-1 RT activity compared to the effects of a non-nucleoside reverse transcriptase inhibitor, efavirenz (24) (Fig. S6*B*). These data suggest that ACAi-001 is not an early-stage inhibitor, as observed with the RT and IN inhibitors. Next, to investigate the effect of ACAi-001 on late-stage inhibition, we determined whether ACAi-001 affected HIV-1 production, including Gag and Gag-pol proteolytic processing and maturation. At 48 h after transfection of pHIV-1_{NL4-3} into 293T cells in the presence of ACAi-001 (50, 20, and 2 μM), Eb (2 μM), or DRV (2 μM), viral production was assessed using ELISA and WB to compare the p24 expression levels in the culture supernatant and those of the intracellular Gag and Gag-pol proteins. ACAi-001 and Eb did not significantly affect viral production, whereas DRV treatment reduced HIV-1 production (Fig. S6*C*). Unlike DRV, ACAi-001 and Eb did not affect Gag proteins in the cells, as shown on the left side of Fig. S6*D*. Additionally, the effect of ACAi-001 on Gag proteolytic processing and maturation of HIV-1 virions was investigated using WB and a TZM-bl assay after purification. ACAi-001 did not affect HIV-1 maturation, as observed via WB with anti-Gag and anti-IN antibodies, similar to the results observed in the DMSO control, as shown in the right panel of Fig. S6*D*. ACAi-001 did not reduce viable virions at 50, 20, and 2 μM as opposed to the effects of DRV (Fig. S6*E*), suggesting that ACAi-001 did not affect HIV-1 production and maturation. Eb binds to cysteines in the CA-CTD and has been reported to inhibit the early-stage, but not the late-stage, of HIV-1 replication (13, 14). Interestingly, premature products such as Gag-pol (p160), Gag (p55), and Gag intermediates were found in purified viruses produced at 2 μM of Eb according to WB with anti-Gag or anti-IN antibodies (Fig. S6*D*), whereas the infectivity of virions containing premature Eb products was not significantly reduced (Fig. S6*E*). These results suggest that Eb affects Gag-pol processing without inhibiting the late-stage of the HIV-1 life cycle. Additionally, ACAi-001 did not significantly impact the early and late stages of the HIV-1 life cycle, in contrast to capsid inhibitors such as Eb and PF74 (16).

ACAi-001 inhibits HIV-1 infection by directly attacking viral particles.
CA proteins constitute the capsid lattice (HIV core) comprising approximately 250 hexamers and 12 pentamers (11). The target cavity is inside the CA hexamer as shown in Fig. 1*B*. To determine the effect of ACAi-001 on viral particles, we examined the direct effect of ACAi-001 on the HIV core in the viral particles. Purified HIV-1 particles were treated with DMSO or ACAi-001 for 24 h. The envelopes of these viruses were removed using Triton X-100, and the envelope-stripped cores were enriched by ultracentrifugation through a continuous 20% to 70% sucrose gradient, as previously reported (25, 26). After ACAi-001 treatment for 24 h, the CA immunogenicity peak, including the HIV core from 50% to 65% sucrose gradient fractions by ELISA, was decreased compared to that following DMSO treatment (Fig. 6*A* and *B*). We also confirmed the state of CA in these sucrose gradient fractions by denaturing WB using a CA anti-polyclonal antibody. In the presence of DMSO, CA monomers were found in the low sucrose fractions and p55 (Gag) were found in the (higher sucrose) HIV-1 core fractions (upper panel of Fig. 6*C*). After treatment with DMSO for 24 h, CA monomer and Gag were also seen in the same fractions (upper panel of Fig. 6*D*). In contrast, upon addition of ACAi-001, CA products slightly appeared in the HIV-1 core fractions compared to after DMSO treatment (lower panel of Fig. 6*C*) and, after treatment with ACAi-001 for 24 h, Gag and various CA products, including aberrant multimerization, were clearly observed in the HIV-1 core fractions (lower panel of Fig. 6*D*) and following direct time-dependent treatment of viral particles with ACAi-001 (Fig. S6*G*). These results indicate that ACAi-001 can directly and covalently bind CA and affect the HIV core in viral particles. Interestingly, when the morphology of mature HIV-1_{NL4-3} virions after incubation with ACAi-001 for 72 h was observed using transmission electron microscopy (TEM) and, the HIV core in the viral particle was remarkably decomposed by ACAi-001 (4.5% normal, 49.2% abnormal, and 44.8% no HIV core structures) compared with the effects of DMSO treatment (72.3% normal, 17.1% abnormal, and 10.6% no HIV core structures) (26) (Fig. 6*E*). These results suggest that ACAi-001 passed through the mature membrane of HIV-1 and directly decomposed the HIV-1 core in the viral particles. Finally, we analyzed the time required for ACAi-001 to exert its anti-HIV-1 activity against viral particles using the TZM-bl assay. HIV-1 particles treated with ACAi-001, PF74, and Eb were incubated for 0, 1, 3, 6, 12, and 24 h and then infected into TZM-bl cells. PF74 and Eb inhibited HIV-1 viral particles in TZM-bl cells without incubation. In contrast, ACAi-001 inhibited HIV-1 viral infection in TZM-bl cells after 3–6 h of treatment, suggesting that ACAi-001 requires at least 3 h of incubation with viral particles to exert anti-HIV-1 activity (Fig. 6*F*, Fig. S6*H*), which is consistent with the appearance of aberrant CA multimerization in the WB results shown in Fig. S2*E*.
In conclusion, ACAi-001 directly and covalently binds to the CA (HIV core) in HIV-1 viral particles and induces aberrant CA multimerization and degradation in a time-dependent manner. This unique mechanism of action of ACAi-001 induces decomposition of the HIV core into viral particles, thereby inhibiting HIV-1 infection. This study demonstrated that ACAi-001, a CA-targeting agent, is a promising covalent anti-CA inhibitor and may be useful for further HIV core research applications.

Discussion
We found that ACAi-001, a unique covalent anti-HIV-1 CA inhibitor that interacts with HIV-1 CA as a targeted covalent inhibitor, induces significant levels of aberrant CA multimerization and degradation. Two covalent-binding structures of ACAi-001 (Fig. 4*A*) and two ACAi-001 binding sites, the ACAi-pocket in the CA-NTD and Cys-pocket in the CA-CTD (Fig. 5*A*), allow aberrant CA multimerization, leading to CA auto-degradation. Crews *et al*. reported interesting compounds that recruit target proteins for ubiquitination and removal by proteasomes (27). Although this approach appears to be attractive for causing target protein degradation, it differs from the mechanism of ACAi-001-induced CA degradation. Misumi *et al*. reported that the uncoating process (28) requires an interaction between CA and peptidyl-prolyl isomerase (Pin1), which specifically recognizes phosphorylated Ser16 and Pro17 (29) overlapping with the ACAi-pocket. Pin1 can transform into an isomer (from cis to trans conformation) by binding to the

phosphorylated Ser/Thr-pro peptide, initiating the uncoating process in the early-stages of HIV-1 infection. Thus, covalent binding of ACAi-001 to Ser16 may also destabilize CA proteins, such as by initiating the uncoating process; however, this requires further research. In contrast, Eb binds covalently to the Cys-pocket (14) (Fig. 2*A* and Fig. 5*A*), which did not induce CA multimerization and degradation (Fig. S3*A*). Collectively, these results indicate that compounds that only covalently bind to the Cys-pocket do not induce CA multimerization and degradation.

When ACAi-001 and HIV-1_{NL4-3} were simultaneously administered to TZM-bl cells, ACAi-001 did not significantly inhibit the early-stage of the HIV-1 life cycle. The aberrant CA multimerization induced by ACAi-001 required 3 h of incubation, and CA degradation occurred after 24 h. The CA multimerization and degradation by ACAi-001 occurred in time- and dose-dependent manners. These results suggest that ACAi-001 does not exert anti-HIV-1 effects until CA multimerization occurs, even though ACAi-001 binds to the ACAi-pocket or Cys-pocket. ACAi-001, which was revealed by our docking simulation to target the ACAi-pocket, may not possess a high level of structural selectivity because ACAi-001 also binds to Cys198 or Cys218 residues in the Cys-pocket, as well as in the ACAi-pocket (Fig. 5). Eb covalently binds to Cys198 or Cys218 in the Cys-pocket (Fig. S5*C*). ACAi-001 also bound to the Cys-pocket (Fig. 5 and S5*C*). However, the anti-HIV-1 mechanism of ACAi-001, which binds to both pockets, differs from that of Eb, which binds only to the Cys-pocket.

In the TZM-bl assay, ACAi-001 also required at least 3 h of incubation to prevent HIV-1 infection via viral particle inhibition (Fig. 6*F*), corresponding to the appearance time of aberrant CA multimerization shown in Fig. S2*D*. These results suggest that the specific structure of ACAi-001, which forms a covalent bond with CA, is among the key modulators of anti-HIV-1 activity. We estimate that ACAi-001, a covalent inhibitor, exerts strong and long-lasting drug effects by irreversibly binding to CA and can react with specific AA residues in CA to achieve selective inhibition. However, the toxicity of ACAi-001 should be confirmed in an *in vivo* model because ACAi-001 may cause unexpected and fatal non-specific reactions by covalently binding to cysteine residues, even if the half-maximal cytotoxic concentration of ACAi-001 is low and ACAi-001 does not affect BSA multimerization and degradation (Table 3 and Fig.S2*H*). In addition, CA forms the HIV core consisting of hexamers and pentamers within the viral particles. As shown in Fig. S6*G*, ACAi-001 directly induced aberrant CA multimerization to the HIV core in the viral particle; however, the ACAi-pocket of one CA and ACAi-pocket or Cys-pocket of the other CA are separated by a large distance to hinge via ACAi-001.

The HIV-1 CA-encoding gene is relatively more well-conserved than the other HIV-1 proteins-encoding genes among various subtypes of HIV-1, including HIV-2 strains (30). This finding is in line with our present data, which demonstrate that ACAi-001 significantly reduced the immunogenicity of CA derived from HIV-1 strains, including various clinically isolated infectious HIV subtypes (Fig. S3*B*) and HIV-2_{ROD} compared to PF74 (Table 2). Therefore, anti-HIV-1 drugs targeting the CA^{WT} of HIV-1 potentially suppress the replication of a wide spectrum of HIV-1/2 subtypes/variants. RT, which synthesizes viral DNA, is highly associated with the uncoating process of CA conical shells (36); however, ACAi-001 did not directly affect the activity of HIV-1 RT (Fig. S6*B*).

This study has other limitations. We generated ACAi-001-resistant HIV-1 cells using a selection assay (31). The cellular DNA of ACAi-001-resistant HIV-1 did not contain any specific mutations in the gag (CA) region (Table S1). This finding suggests that ACAi-001 is not a strong anti-CA compound and may use an alternative mechanism, such as a non-specific reaction to HIV-1 viral particles. In addition, co-crystallization and X-ray diffraction analysis are frequently used to determine the detailed binding profile between a certain compound/drug and its target; however, co-crystallization of CA decomposer and CA may be challenging because of the nature of ACAi-001 as a CA decomposer.

Taken together, these findings suggest that anti-HIV-1 compounds that covalently bind to specific sites of CA (ACAi- and/or Cys-pockets) serve as targets for the multimerization and decomposition of CA proteins, which could lead to effective intervention in HIV-1 replication.

Materials and Methods

Cells.
MT-2 and MT-4 cells (Japanese Collection of Research Bioresources Cell Bank; JCRB Cell Bank, Japan) were cultured in RPMI1640 medium (Gibco, Grand Island, NY, USA) supplemented with fetal bovine serum (Gibco), penicillin, and kanamycin. 293T and COS7 cells obtained from the JCRB Cell Bank and TZM-bl cells obtained from the NIH AIDS Research and Reference Reagent Program were cultured in low-glucose Dulbecco's Modified Eagle Medium supplemented with L-glutamine, phenol red (Fujifilm Wako Pure Chemical Corporation, Osaka, Japan), fetal bovine serum, penicillin, and kanamycin.

Plasmids.
The CA-encoding plasmids expressed in cells were generated as follows: pCMV-Myc (Takara Bio, Shiga, Japan) was digested by ApaI/XhoI to remove the Myc epitope and linearize the vector. The CA fragment of pNL4-3 was amplified by polymerase chain reaction, and the fragment was introduced into linearized pCMV using an in-fusion enzyme (Clontech Laboratories, Mountain View, CA, USA). The CA-encoding plasmid expressed in *E. coli* was produced by amplifying a CA fragment from pNL4-3 into a linearized pET30a vector with or without His (Novagen-Merck KGaA, Darmstadt, Germany), producing pET30a CA or pET30a CA His+ vectors. Site-directed mutagenesis was performed using PrimeSTAR® Max (Takara Bio) to introduce S16E, C198A/C218A, or S16E/C198A/C218A mutations into the pET30a CA vector, producing pET30a CA^{S16E}, $CA^{C198A/C218A}$, and $CA^{S16E/C198A/C218A}$ vectors, respectively.

Viruses.
The HIV-1 laboratory strain HIV-1_{LAI} was propagated in MT-2 cells. HIV-1_{NL4-3} and G glycoprotein of vesicular stomatitis virus (VSV-G) HIV-1_{dENV} were produced by transfecting 293T cells with the pNL4-3 or pCMV-VSV-G vector (Addgene, Watertown, MA, USA) plus pNL4-3 $_{dENV}$, respectively (13). HIV-$1_{97UG029}$, HIV-$1_{92UG037}$, HIV-$1_{97ZA003}$, and HIV-1_{Ba-L} were provided by the National Institutes of Health AIDS Reagent Program. Virus samples were analyzed using an HIV-1 p24 ELISA on a Lumipulse G1200 (Fujirebio, Inc., Malvern, PA, USA) and normalized to determine the virus concentration. Viral samples were solubilized with 0.5% of Triton X, and p24 levels were measured using an HIV-1 p24 ELISA on a Lumipulse G1200 and normalized to determine the virus concentration.

CA preparations expressed in the cells.
We prepared the lysates of COS-7 cells expressing CA^{WT} by transfection, then divided the cell lysates equally into four different tubes containing 100 μM of ACAi-001. One tube was stored at -80°C immediately after dividing the cell lysates, and the other tubes were incubated at 37°C for 24, 48, and 72 h. The %CA at each time point in the ELISA of Lumipulse G1200 was calculated as a relative percentage.

Protein expression and purification.
The procedure for purifying CA proteins has been described previously (5, 13). CA proteins were produced from pET30a CA introduced into *E. coli* Rosetta™ (DE3) pLysS competent cells (Novagen, Madison, WI, USA) grown in LB medium supplemented with K and chloramphenicol at 37°C and induced with Isopropyl β-D-1-thiogalactopyranoside for 3–5 h at 37°C. The bacterial cells, including CA, were resuspended and sonicated. Lysates were cleared by centrifugation. After adding 5 M NaCl to the supernatant, the samples were cleared by centrifugation. The precipitate was resuspended in CA buffer (150 mM NaCl, 5 mM βME, 50 mM Tris-HCl, pH 7.5). The sample was precleared and then filtered through a 0.45 μm filter. The CA proteins were loaded onto a HiLoad 16/60 Superdex 200 column (GE Healthcare, Little Chalfont, UK) and eluted using an AKTA Prime Plus (GE Healthcare). The CA monomer fractions were concentrated in CA buffer using an Amicon Ultra-10K device (Merck Millipore, Billerica, MA, USA). The protein concentration was determined using a BCA Protein Assay Reagent Kit (Thermo Fisher Scientific, Waltham, MA, USA) and stored at -80°C.

TZM-bl assay.
The TZM-bl assay was performed as previously described (13). TZM-bl cells were obtained from the NIH AIDS Research and Reference Reagent Program. Briefly, 50 µL of cells (10^5/mL) were seeded into black 96-well plates and incubated for 24 h in the presence of 5% CO_2 at 37°C. Diluted drugs mixed with viruses (final concentration: 50 ng/mL) plus diethyl aminoethyl-dextran (final concentration: 25 µg/mL) were added to the cells (total final volume: 200 µL). After 48 h of incubation at 37°C in the presence of 5% CO_2, the supernatant was removed, and lysis buffer was added to the samples. After shaking the samples for 10 min, D-luciferin was added to each well. After shaking, luciferase intensity was measured using a FluoSTAR Omega (BMG Labtech GmbH, Ortenberg, Germany).

RT assay.
A colorimetric RT assay was performed (Reverse Transcriptase Assay Colorimetry; Roche, Basel, Switzerland). Briefly, recombinant HIV-1 RT was added to the test compounds dissolved in lysis buffer and then incubated at 37°C and 5% CO_2 for 3–4 h. After washing, peroxidase-conjugated anti-digoxigenin antibody solution was added to the samples and incubated at 37°C with 5% CO_2 for 1 h. After washing, ABTS peroxidase substrate solution with an enhancer was added to each sample. The optical density was measured at 405 nm using a Versamax microplate reader (Molecular Devices, Sunnyvale, CA, USA).

WB.
WB was performed as described previously (32). Briefly, 293T cells were plated and incubated at 37°C in 5% CO_2 for 24 h. The cells were transfected with pNL4-3 vectors using Attractene transfection reagent (QIAGEN, Hilden, Germany). After 8 h, the medium was changed and tested compounds were added, followed by incubation for 48 h. The viruses were filtered through a 0.20 nm filter, partially purified by ultracentrifugation in 15% sucrose-phosphate-buffered saline (PBS), normalized to the p24 levels, and stored in PBS at -80°C. The cells were lysed in M-per buffer (Thermo Fisher Scientific) supplemented with Halt Protease Inhibitor Cocktail (Thermo Fisher Scientific). The samples were titrated using a BCA Protein Assay Kit or p24 ELISA on a Lumipulse G1200 and stored at -80°C. The samples were prepared using NuPAGE LDS Sample Buffer (Thermo Fisher Scientific), separated by SDS-PAGE (5–20% Extra PAGE One Precast Gel; Nacalai Tesque, Kyoto, Japan), and transferred onto a nitrocellulose membrane. The samples were detected with anti-CA antibodies (monoclonal antibody, ab63913; Abcam, Cambridge, UK, and polyclonal antibody, Cat# 13-203-000, RRID: AB 1929205; Advanced Biotechnologies, Eldersburg, MD, USA), anti-HIV-1 Gag (p55 + p24 + p17) antibody (ab63917; Abcam), anti-HIV-1 IN antibody (ab66645; Abcam), BSA antibody (2A3E6, Santa Cruz Biotechnology, Dallas, TX, USA), secondary mouse or rabbit antibody (MBL Co., Ltd., Tokyo, Japan) and anti-beta actin antibody (horseradish peroxidase-conjugated) (ab49900; Abcam), and then visualized with SuperSignal WestPico chemiluminescent substrates (Thermo Fisher Scientific).

SEC.
Recombinant CA proteins were analyzed using a Cosmosol-120 column (Nacalai Tesque) at 1.0 ml/min in PBS (pH 7.4) (13, 33). CA proteins (40 µM) treated with DMSO and ACAi-001 in sample buffer (ammonium bicarbonate (A.B.), pH 7.5) were evaluated on an Agilent Technologies 1220 Infinity LC system (Santa Clara, CA, USA) for SEC and were detected at an optical density of 280 nm. The column was calibrated using standard proteins containing chicken ovalbumin (44 KDa) and horse myoglobin (17 KDa). All procedures were performed at 4°C to the extent possible.

CA multimerization assay.
CA multimerization assays were performed as previously described (13, 18). Compounds and drugs were added to CA proteins (30 µM) in 50 mM phosphate buffer at pH 8.0 supplemented with 50 mM NaCl. Capsid assembly was initiated by adding 50 mM sodium phosphate (pH 8.0)

supplemented with 5 M NaCl. The optical density at 350 nm was measured every 5 min for 2 h using the FluoSTAR Omega.

Differential scanning fluorimetry.
The differential scanning fluorimetry method has been described previously (13, 19). Briefly, recombinant CA proteins (25 µM) were prepared in PBS. After the CA treatment of the tested compounds for 8–12 h at 25°C SYPRO Orange (Life Technologies, Carlsbad, CA, USA) was added to the samples (final concentration of SYPRO Orange: 5×). The samples were successively heated from 25°C to 95°C, and the increasing fluorescence intensities were measured with a Real-time PCR system 7500 Fast (Applied Biosystems, Foster City, CA, USA). Data are expressed as a relative ratio between the minimum and maximum intensity of SYPRO Orange detected from 25°C to 95°C for each sample.

Electrospray ionization-MS and LC-MS.
The electrospray ionization-MS protocol has been described previously (13, 33). Briefly, the MS spectra of CA in the presence of ACAi-001 were obtained using an electrospray ionization quadrupole time-of-flight (QTOF) mass spectrometer (Impact II, Bruker Daltonics, Billerica, MA, USA). Each sample solution under native conditions was introduced to the ESI-QTOF mass spectrometer through an infusion pump at a flow rate of 3.3 µL/min. The denatured samples were analyzed using a QTOF mass spectrometer equipped with a Captive Spray electrospray ionization platform with LC (Ultimate 3000 HPLC, Thermo Fisher Scientific). The following ion source parameters were applied: dry heater: 150˚C, dry gas: 8.0 L/min, capillary voltage: 1000 V, end plate offset: -500 V. MS scans were acquired at a spectra rate of 1 Hz at a mass range from 100 to 3000 m/z. MW by protein deconvolution was determined using Data Analysis 4.4 (Bruker Daltonics). The MW of the CA proteins was calculated using the Peptide Mass Calculator v3.2 (http://rna.rega.kuleuven.be/masspec/pepcalc.htm).

Viral core analysis.
HIV-1 viral core analysis using sucrose density gradient centrifugation was performed as previously described (25, 26). Briefly, HIV-1 virions were produced in the presence of DMSO or ACAi-001 and concentrated in 400 µL on a 15% sucrose cushion by ultracentrifugation at 35,000 rpm for 30 min at 4°C in an SW55 rotor of an Optima X (Beckman Coulter, Brea, CA, USA). Concentrated virions were envelope-stripped with 0.2% Triton-X for 2 min at room temperature. Lysed virions were loaded onto 25% to 70% linear sucrose density gradients in STE buffer (10 mM Tris-HCl pH 7.5, 100 mM NaCl, 1 mM EDTA) and ultracentrifuged at 28,500 rpm for 16 h at 4°C in SW55 rotor. Eleven fractions per 400 µL were collected from the top of the samples and the viral core was examined by p24 ELISA and immunoblotting with anti-CA antibody.

TEM.
Viruses were produced by transfection with pNL4-3 into 293T cells. After 12 h of incubation, the cell supernatant was replaced with fresh medium. After 48 h of incubation, the supernatants were filtered through a 0.45-m filter, and ultracentrifugation was performed using a model 7780 centrifuge (Kubota, Osaka, Japan) at 22,000 rpm for 12 h at 4°C. Virus pellets were resuspended in PBS and treated with DMSO or 100 µM of ACAi-001 for 72 h at 37°C. The ultracentrifugation step was repeated, and the virus pellets were dissolved in a small amount of buffer (2% glutaraldehyde in 0.1 M phosphate buffer, pH 7.4), and shipped to Tokai Electron Microscopy Inc. (Aichi, Japan). Digital images (3,296 × 2,472 pixels) were taken with a charge-coupled device camera (EM-14830RUBY2; JEOL Ltd., Tokyo, Japan). Over 100 virus images for each sample were classified as three types of (no, abnormal, or normal) HIV cores in the viral particles.

Drug susceptibility assay.
The susceptibility of HIV-1_{LAI} and HIV-2_{ROD} to ACAi-001 and control drugs was determined as previously described (34). Briefly, MT-2 cells (10^4/mL) were exposed to 100× of the 50% tissue culture infectious dose ($TCID_{50}$) of HIV-1_{LAI} or HIV-2_{ROD} in the presence or absence of various

concentrations of compounds in 96-well plates and incubated at 37°C with 5% CO_2 for 7 days. After incubation, 100 µL of the medium was removed from each well, and MTT solution was added to each well, followed by incubation at 37°C for 2–4 h. After incubation to dissolve the formazan crystals, acidified isopropanol containing 4% (v/v) Triton X-100 was added to each well, and the optical density was measured using a kinetic microplate reader (Vmax; Molecular Devices). All assays were performed in duplicate. The 50% cytotoxic concentration of compounds/drugs for each cell line was also evaluated using an MTT assay. To determine the sensitivity of primary HIV-1 isolates to the compounds, phytohemagglutinin-stimulated peripheral blood mononuclear cells (10^6/mL) were exposed to 50× of the $TCID_{50}$ of each primary HIV-1 isolate and cultured in the presence or absence of various drug concentrations in 10-fold serial dilutions in 96-well plates. To determine the drug susceptibility of laboratory HIV-1 strains, MT-4 cells were used as target cells as previously described (35), with minor modifications. Briefly, MT-4 cells (10^5/mL) were exposed to 100× of the $TCID_{50}$ of drug-resistant HIV-1 strains in the presence or absence of various concentrations of compounds and then incubated at 37°C. On day 7 of culture, the supernatants were harvested, and p24 protein levels were determined using the Lumipulse G1200. Drug concentrations that suppressed the production of p24 Gag protein by 50% (50% effective concentration) were determined by comparison with p24 levels in drug-free control cell culture. The phytohemagglutinin-stimulated peripheral blood mononuclear cells were derived from a single donor in each independent experiment.

Compounds.
ACAi-001 was purchased from ChemBridge (San Diego, CA, USA), or ACAi-001, ANS-1028, and ANS-1050 were synthesized by a co-author (see Supplementary Methods); RAL was from Selleck Chemicals (Houston, TX, USA); zidovudine, ABC, 3TC, PF74, and efavirenz were from Sigma-Aldrich (St. Louis, MO, USA); and Eb was from AdipoGen Life Sciences (Füllinsdorf, Switzerland). The drugs were diluted in DMSO or methanol and stored in a freezer or deep freezer prior to use.

Acknowledgments.
This work was supported by the Japan Society for the Promotion of Science, KAKENHI, grant number 23K24379 (M.A.).

References

1. L. E. Henderson, *et al*., Gag precursors of HIV and SIV are cleaved into six proteins found in the mature virions. *J Med Primato*l. **19**, 411–9 (1990).
2. L. E. Henderson, *et al*., Gag proteins of the highly replicative MN strain of human immunodeficiency virus type 1: posttranslational modifications, proteolytic processings, and complete amino acid sequences. *J Virol*. **66**, 1856–65 (1992).
3. B. K. Ganser-Pornillos, A. Cheng, M. Yeager, Structure of full-length HIV-1 CA: a model for the mature capsid lattice. *Cell.* **131** 70–9 (2007).
4. J.A. Briggs *et al*., Structural organization of authentic, mature HIV-1 virions and cores. *EMBO J*. **22**, 1707–15 (2003).
5. M. Amano *et al*., Amino-acid inserts of HIV-1 capsid (CA) induce CA degradation and abrogate viral infectivity: Insights for the dynamics and mechanisms of HIV-1 CA decomposition. *Sci Rep.* **9** 9806 (2019).
6. E. de. Vita, 10 years into the resurgence of covalent drugs*. Future Med Chem*. **13** 2 (2021).
7. J. Singh, R. C. Petter, T. A. Baillie, A. Whitty, The resurgence of covalent drugs. *Nat Rev Drug Discov*. **10** 4 (2011).
8. X. Xie *et al*., Recent advances in targeting the "undruggable" proteins: from drug discovery to clinical trials. *Signal Transduct Target Ther*. **8** 335 (2023).
9. B. R. Lanning *et al*., A road map to evaluate the proteome-wide selectivity of covalent kinase inhibitors. *Nat Chem Biol*. **10** 760–67 (2014).

10. M. E. Flanagan *et al*., Chemical and computational methods for the characterization of covalent reactive groups for the prospective design of irreversible inhibitors. *J Med Chem*, **57** 10072–9 (2014).
11. O. Pornillos *et al*., X-ray structures of the hexameric building block of the HIV capsid. Cell. **137** 1282–92 (2009).
12. K. Peden, M. Emerman, L. Montagnier, Changes in growth properties on passage in tissue culture of viruses derived from infectious molecular clones of HIV-1_{LAI}, HIV-1_{MAL}, and HIV-1_{ELI}. Virology. **185** 661–72 (1991).
13. T. Chia, *et al.*, A small molecule, ACAi-028, with anti-HIV-1 activity targets a novel hydrophobic pocket on HIV-1 capsid. *Antimicrob Agents Chemother.* **65** e0103921 (2021).
14. S. Thenin-Houssier, *et al*., Ebselen, a small-molecule capsid inhibitor of HIV-1 replication. *Antimicrob Agents Chemother* **60** 2195–208 (2016).
15. M. Markowitz *et al*., Antiretroviral activity, pharmacokinetics, and tolerability of MK-0518, a novel inhibitor of HIV-1 integrase, dosed as monotherapy for 10 days in treatment-naive HIV-1-infected individuals. *J Acquir Immune Defic Syndr* **43** 509–15 (2006).
16. W. S. Blair *et al*., HIV Capsid is a Tractable Target for Small Molecule Therapeutic Intervention. *PLoS Pathog* **6** e1001220. (2010).
17. J. O. Link *et al*., Clinical targeting of HIV capsid protein with a long-acting small molecule. *Nature* **584** 614–618 (2020).
18. J. Lanman, J. Sexton, M. Sakalian, PE. Jr. Prevelige, Kinetic analysis of the role of intersubunit interactions in human immunodeficiency virus type 1 capsid protein assembly in vitro. *J Virol* **76** 6900–8 (2002).
19. F. H. Niesen, H. Berglund, M. Vedadi. The use of differential scanning fluorimetry to detect ligand interactions that promote protein stability. *Nat Protoc* **2** 2212–21 (2007).
20. F. Li *et al*., PA-457: a potent HIV inhibitor that disrupts core condensation by targeting a late step in Gag processing. *Proc Natl Acad Sci U S A*. **23** 13555–60 (2003).
21. D. Schaefer, X. Cheng, Recent Advances in Covalent Drug Discovery. *Pharmaceuticals (Basel)* **16** 663 (2023).
22. Y. Koh *et al*., Novel bis-Tetrahydrofuranylurethane-Containing Nonpeptidic Protease Inhibitor (PI) UIC-94017 (TMC114) with Potent Activity against Multi-PI-Resistant Human Immunodeficiency Virus In Vitro. *Antimicrob Agents Chemother* **47** 3123–29 (2003).
23. H. Mitsuya *et al*., 3'-Azido-3'-deoxythymidine (BW A509U): An antiviral agent that inhibits the infectivity and cytopathic effect of human T-lymphotropic virus type III/lymphadenopathy-associated virus in vitro. *Proc Natl Acad Sci U S A* **82** 096–100 (1985)
24. S. D. Young *et al*., L-743,726 (DMP-266): a novel, highly potent nonnucleoside inhibitor of the human immunodeficiency virus type 1 reverse transcriptase. *Antimicrob Agents Chemother* **39** 2602–5 (1995)
25. S. Tang *et al*., Human immunodeficiency virus type 1 N-terminal capsid mutants containing cores with abnormally high levels of capsid protein and virtually no reverse transcriptase. *J Virol* **77** 12592–602 (2003).
26. J. Jiang *et al*., The interdomain linker region of HIV-1 capsid protein is a critical determinant of proper core assembly and stability. *Virology* **421** 253–65 (2011).
27. M. Békés, D.R. Langley, C.M. Crews, PROTAC targeted protein degraders: the past is prologue. *Nat Rev Drug Discov* **21** 181–200 (2022).
28. D. J. Rawle, D. Harrich, Toward the "unravelling" of HIV: Host cell factors involved in HIV-1 core uncoating Introduction to HIV-1 uncoating: Down the rabbit hole. *PLoS Pathog* **14** e1007270 (2018).
29. S. Misumi *et al*., Uncoating of human immunodeficiency virus type 1 requires prolyl isomerase Pin1. *J Biol Chem* **285** 25185–95 (2010).
30. G. Li *et al*., Functional conservation of HIV-1 Gag: implications for rational drug design. *Retrovirology* **10** 126 (2013).

31. M. Amano *et al*., GRL-0519, a novel oxatricyclic ligand-containing nonpeptidic HIV-1 protease inhibitor (PI), potently suppresses replication of a wide spectrum of multi-PI-resistant HIV-1 variants in vitro. *Antimicrob Agents Chemother* **57** 2036–46 (2013).
32. T. Nakamura, *et al*., A conformational escape reaction of HIV-1 against an allosteric integrase inhibitor. *J Virol* **94** e00486–20 (2020).
33. T. Nakamura, *et al*., Conversion of raltegravir carrying a 1,3,4-oxadiazole ring to a hydrolysis product upon pH changes decreases its antiviral activity. *PNAS Nexus* **3** pgad446 (2023).
34. M. Amano *et al*., Novel Central Nervous System (CNS)-Targeting Protease Inhibitors for Drug-Resistant HIV Infection and HIV-Associated CNS Complications. *Antimicrob Agents Chemother* **63** e00466–19 (2019).
35. M. Amano *et al*., A novel bis-tetrahydrofuranylurethane-containing nonpeptidic protease inhibitor (PI), GRL-98065, is potent against multiple-PI-resistant human immunodeficiency virus in vitro. *Antimicrob Agents Chemother* **51** 2143-55 (2007).
36. R.C. Burdick *et al*., HIV-1 uncoating requires long double-stranded reverse transcription products. *Sci Adv.* **10** eadn7033 (2024).
37. F. Clavel *et al*., Isolation of a new human retrovirus from West African patients with AIDS. Science. **233** 343–6 (1986).

Figures and Tables

Fig. 1. ACAi-001 was selected by a targeting hydrophobic cavity near Arg18-Thr19 on the surface of CA-N-terminal domain (NTD).
A) Location of Arg18-Thr19 is shown in red; the yellow square line indicates the targeting hydrophobic cavity in the CA-NTD, and hydrophobic regions are shown in blue. **B**) Location of the identified target cavity of the CA-NTD in a CA hexameric state is illustrated from the top view and from the side view. **C**) Chemical structure of ACAi-001 is shown on the left side. ACAi-001 was simulated to interact strongly with Ala14, Ser16, and Glu45, constituting the target cavity by docking simulation. Docking simulations were performed with SeeSAR and FlexX version 10 (BioSolveIT GmbH, Sankt Augustin, Germany).

Fig. 2. CA multimerization and degradation profile induced by ACAi-001.
A) In the denatured state of liquid chromatography-mass spectrometry (LC-MS), black arrows represent CA monomer (10 µM) peaks of the charged ions. Light and normal blue arrows represent one and two ACAi-001 (50 µM) binding to the CA monomer, respectively. Yellow and orange arrows represent one and two Eb (50 µM) binding to the CA monomer, respectively. The molecular weight (MW) calculated from charged ions of the CA plus the drugs is shown as a deconvolution on the right side. **B**) CA treated with dimethyl sulfoxide (DMSO; 1%), ACA-001 (100 µM), raltegravir (RAL; 100 µM), PF74 (20 µM), and ACAi-028 (20 µM) for 0 h incubation is shown on the left side, and that for 72 h of incubation is shown on the right side. Triangular arrows indicate the putative MW size of the CA monomer (Mo), dimer (Dim), timer (Tri), and tetramer (Tet). **C**) Size-exclusion chromatography (SEC) analysis of CA proteins. The CA peaks treated with DMSO and ACAi-001 (100 µM) for 0 h of incubation are shown on the left side and those for 72 h of incubation are shown on the right side. **D**) CA multimerization assay was performed by addition of high-sodium buffer after 24 h incubation of ACAi-001 (2, 20, and 200 µM) and RAL (100 µM) with CA proteins under low-sodium conditions. The turbidity of the mixtures was measured at an OD_{350} for 120 min. **E**) Differential scanning fluorimetry was performed using SYBR-Orange dye in the presence of DMSO (black circle), different concentrations of ACAi-001 (2, 20, and 200 µM; blue circles), and RAL (100 µM; green circle). A graphical representation of Tm changes (ΔTm 50) of CA proteins from 0 to 72 h of incubation with DMSO, ACAi-001, and RAL is shown on the right side. All assays were performed in triplicate, and error bars indicate ± SD from at least three independent experiments. Statistical significance was determined by Student's *t*-test (*, $P < 0.05$).

Fig.3. Detection of ACAi-001-induced CA multimerization and degradation in cellular expression lysates.
A) Effects of CA cell lysates treated with dimethyl sulfoxide (DMSO) (black circles) or ACAi-001 (blue circles) for 24, 48, and 72 h at 37°C were measured by automated p24 enzyme-linked immunosorbent assay (ELISA) on the left side and western blotting (WB) on the right side. **B**) Those treated with DMSO or PF74 are shown by automated p24 ELISA. **C**) Effects of HIV-1_{NL4-3} lysates treated with DMSO (black circles) or ACAi-001 (blue circles) for 24, 48, and 72 h at 37°C were measured by p24 ELISA on the left side and WB on the right side. **D**) Those treated with DMSO, bevirimat (BVM), or PF74 are shown. **E**) Dose-dependent effects of ACAi-001 (1, 10, and 100 µM) at 37°C on CA cell lysates are visualized by p24 ELISA. **F**) Effects of DMSO (black circles) or ACAi-001 (blue circles) incubation for 24, 48, and 72 h at 37°C on HIV-2_{ROD} lysates were measured by p24 ELISA.

Fig. 4. Putative covalent reactions of ACAi-001 to CA proteins.
A) Putative ACAi-001 structural changes and reactions to CA. ACAi-001 contains hydroquinone and hydrazide moieties, which are covalently reactive moieties. Upon oxidation, the hydroquinone moiety is converted to *p*-benzoquinone surrounded by the dashed blue square, which can form a covalent bond to sulfur-containing amino acids such as cysteine in a CA. The hydrazide moiety is converted to the nucleophile (Nu-H) structure surrounded by the dashed red square, which can

covalently bond to the other CA. A schematic illustration of the aberrant CA multimerization induced by ACAi-001 is shown in the gray square. **B**) Dose-dependent aberrant CA multimerization and degradation induced by ACAi-001 (2, 20, and 200 µM) are shown on the left side after 24 h incubation in the reaction buffer, and those in the reaction buffer supplemented with a reducing agent, 10 mM of 2-mercaptoethanol (βME), are shown on the right side. **C**) CA multimerization and degradation induced by ACAi-001 (100 µM), ANS-1028 (100 µM), ANS-1050 (100 µM), PF74 (100 µM), and ebselen (Eb; 100 µM) are shown using western blotting (WB) with anti-p24 antibody. The chemical structures of ANS-1028 and ANS-1050, which converted the p-hydroquinone of ACAi-001 to the individual phenols, which are surrounded by the dashed blue square, PF74, and Eb are shown on the right side. All assays were performed independently at least twice, and the representative data are shown.

Fig. 5. ACAi-001 interacts with Ser16 in the CA-N-terminal domain (NTD) and Cys198 and 218 in the CA-C-terminal domain (CTD).
A) S16 residue (red) is located in the ACAi-001 target pocket, the ACAi-pocket shown in the red circle, of the CA-NTD. Residues C198 and C218 (blue) are located in the Cys-pocket of the CA-CTD. A WebLogo 3 visualization (http://weblogo.threeplusone.com/create.cgi) depicts the amino acid frequencies in the CA-NTD (residues 1-50) and CA-CTD (residues 182-231) regions, generated from 12,261 sequences across all HIV-1 subtypes from the Los Alamos HIV sequence database (filtered Web alignment, 2022). Ser16, Cys198, and Cys218 are marked with red square boxes, with their percentage consensus (determined by Jalview 2.11.1.4, http://www.jalview.org) shown above. **B**) Multimers of CA^{WT}, CA^{S16E}, $CA^{C198A/C218A}$, or $CA^{S16E/C198A/C218A}$ induced by ACAi-001 (100 µM) after incubation for 24 h are shown by SEC analysis. **C**) Aberrant CA multimerization carrying S16E, C198A/C218A, or S16E/C198A/C218A induced by ACAi-001 (5, 10, and 20 µM) was visualized by western blotting (WB). The gray arrows of Mo, Dim, Tri, and Tet indicate the MW sizes of CA monomer, dimer, trimer, and tetramer, respectively. **D**) Binding of ACAi-001 to CA^{WT} and $CA^{S16E/C198A/C218A}$ were investigated by liquid chromatography-mass spectrometry (LC-MS) in the denatured state. The calculated molecular weights (MWs) from these ion peaks are displayed in the right deconvolution panel. All assays were performed independently at least twice, and representative data are shown.

Fig. 6. ACAi-001 directly and covalently targets HIV-1 viral particles.
Viral core analyses of purified HIV-1 were performed using sucrose density gradient fraction from 20% to 70% after treatment with ACAi-001 for 0 h **A and C**) or 24 h **B and D**). The p24 values and CA proteins in these fractions were examined using enzyme-linked immunosorbent assay (ELISA) and western blotting (WB) with anti-CA antibody as shown as **A**) and **B**), respectively. Those treated with dimethyl sulfoxide (DMSO) or 100 µM of ACAi-001 for 24 h are shown as **C**) and **D**), respectively. **E**) Transmission electron microscopy (TEM) analysis was used to observe the purified viruses treated with DMSO or 100 µM of ACAi-001 for 72 h at 37°C. The viral morphology with no, abnormal, or normal core in the viral particles was compared as a ratio. **F**) Viral particle inhibition was determined by measuring the infectivity of VSV-G HIV-$1_{\Delta ENV}$ treated with DMSO, ACAi-001 (50 µM), PF74 (10 µM), and ebselen (Eb; 10 µM) incubated for 0, 1, 3, 6, 12, and 24 h using TZM-bl cells. Two or three independent experiments were performed, error bars indicate ± SD, and the representative data are shown.

Table 1. Factors and characteristics of drugs in oral bioavailability prediction.

Drugs	MW (Da)	LogP	CLogP	LogS	TPSA ($Å^2$)	pKa
ACAi-001	339.32	2.59	0.61	93.62	-4.75	7.72
PF74	453.59	4.39	5.18	43.86	-6.42	N/A
LEN	968.28	-12.72	3.47	152.97	-12.72	N/A

*Topological Polar Surface Area, TPSA
LogP is the octanol/water partition coefficient index of fat and water solubility. CLogP is one of the predicted values of LogP; a larger value indicates higher fat solubility. LogS is an index of a drug's water solubility; a larger value indicates higher water solubility. TPSA is an index obtained by approximating the polarized surface area of a molecular surface; the greater the polarized surface area of a drug, the more difficult it is for the drug to physically penetrate the cell membrane. pKa, acid dissociation constant. Data are calculated and predicted by ChemDraw ver.17 (Perkin Elmer). HIV capsid inhibitor; PF74 and Lenacapavir (LEN). N/A, not available.

Table 2. Anti-HIV-1 activity of ACAi-001 against HIV-1, HIV-2, or HIV-1 capsid inhibitor (BVM)-resistant variant.

Virus	Cells	EC_{50} (μM)			
		ACAi-001	ABC	3TC	PF74
$HIV\text{-}1_{LAI}$	MT-2	0.5 ± 0.1	3.3 ± 0.1	2.9 ± 0.3	0.34 ± 0.05
$HIV\text{-}2_{ROD}$	MT-2	1.6 ± 0.3	4.0 ± 0.9	>10	>10
$HIV\text{-}1_{BVM}{}^{R}$	MT-4	2.0 ± 0.3	>10	4.2 ± 0.1	>10

MT-2 cells (10^4/ml) were exposed to 100 $TCID_{50}$ of $HIV\text{-}1_{LAI}$ or $HIV\text{-}2_{ROD}$ and cultured in the presence of various concentrations of each compound, and the EC_{50} (50% effective concentration) values were determined using the MTT assay. For $HIV\text{-}1_{BVM}{}^{R}$, an HIV-1 variant resistant to the HIV-1 capsid inhibitor bevirimat (BVM) generated in the BVM drug selection experiment, EC_{50} values were determined using MT-4 cells as target cells. MT-4 cells (10^5/ml) were exposed to 100 $TCID_{50}$s of $HIV\text{-}1_{BVM}{}^{R}$, and the inhibition of p24 Gag protein production by each drug was used as the endpoint. All assays were performed in duplicate, and the data shown represented mean values (± S.D.) derived from the results of two or three independent experiments.
The following compounds were used as controls: HIV-1 reverse transcriptase inhibitor abacavir (ABC), lamivudine (3TC), HIV-1 capsid inhibitor, and PF74.

Table 3. Cytotoxicity of ACAi-001 against various human cell-lines.

Cells	Origin	CC_{50} (μM)			
		ACAi-001	AZT	3TC	PF74
Li-7	Human hepatocyte	>100	>100	>100	>100
HLE	Human hepatocyte	>100	>100	n.d.	>100
HepG2	Human hepatocyte	>100	n.d.	>100	>100
YSCCC	Human bile-duct cell	>100	>100	>100	>100
HEK293	Human kidney cell	>100	>100	n.d.	>100
MT-2	Human lymphocyte	45.6	>100	n.d.	>100
MT-4	Human lymphocyte	44.8	>100	n.d.	>100

Cells were incubated with serially diluted respective compounds for 1 week before cytotoxicity was quantified using the MTT assay. The following compounds were used as controls HIV-1 reverse transcriptase inhibitors; zidovudine (AZT) and lamivudine (3TC), HIV-1 capsid inhibitor; PF74.

illustration

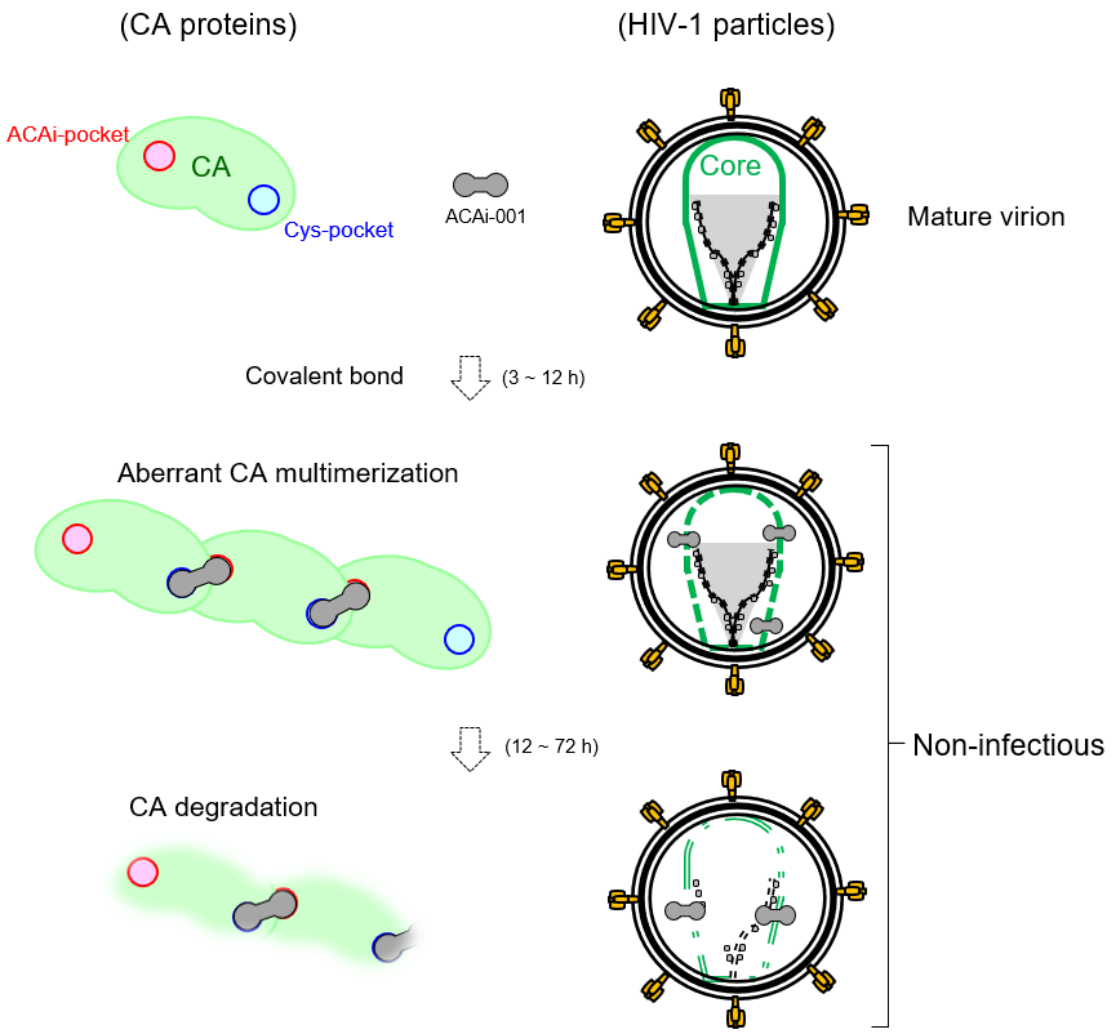

Fig. 1

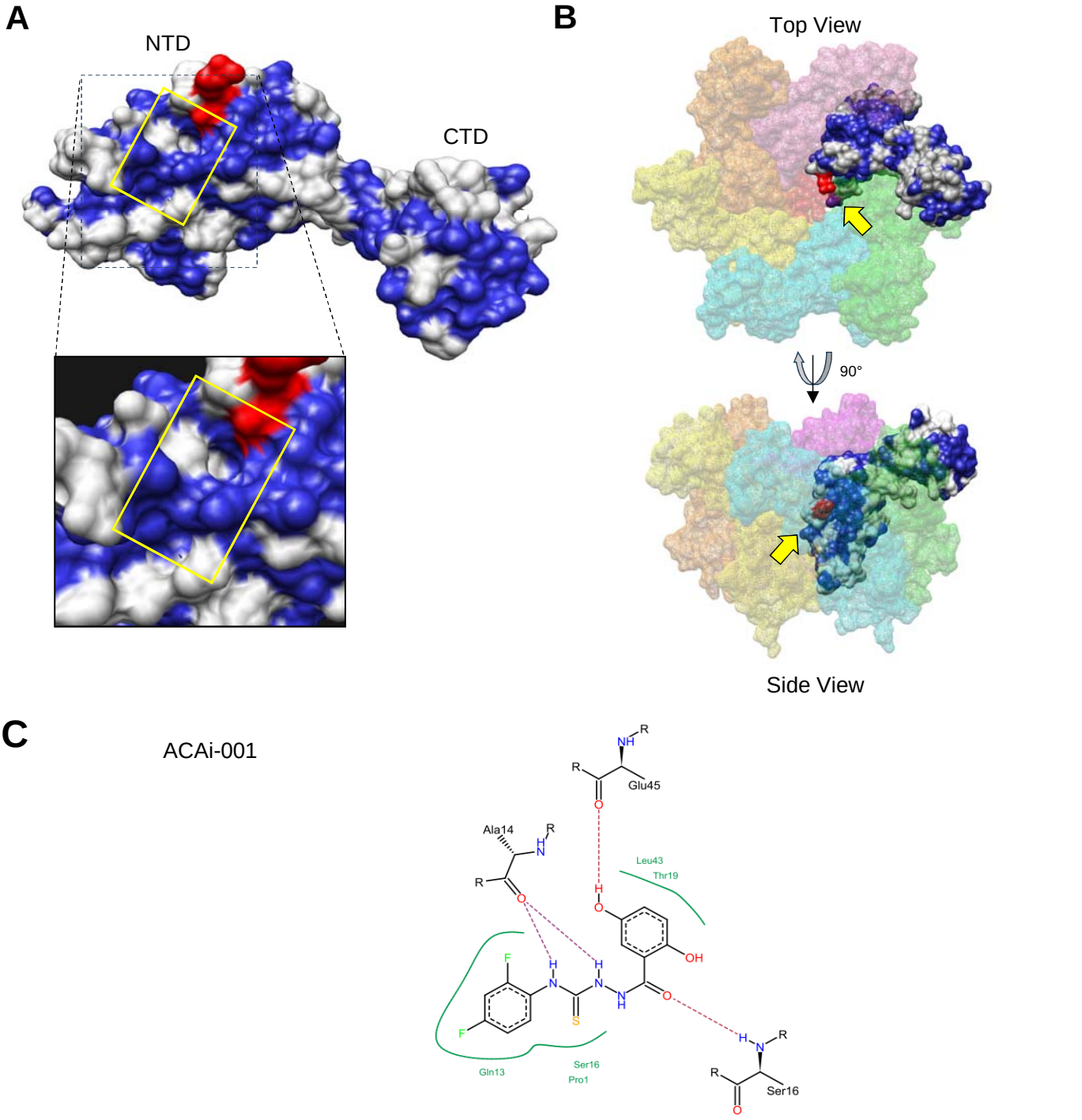
A
NTD
CTD
B
Top View
90°
Side View
C
ACAi-001
Glu45
Ala14
Leu43
Thr19
OH
Gln13
Ser16
Pro1
Ser16

Fig. 2

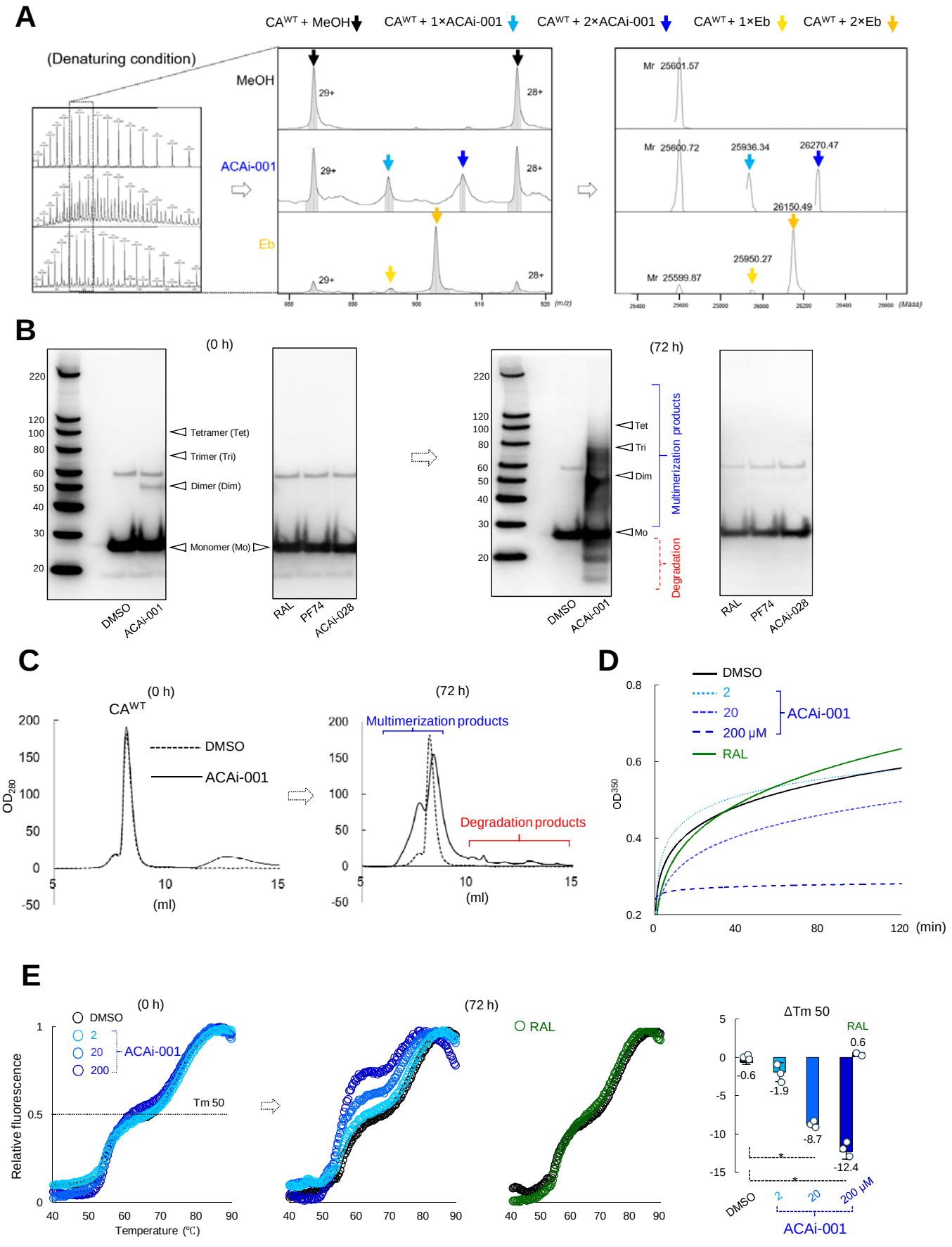
A
CAWT + MeOH
CAWT + 1×ACAi-001
CAWT + 2×ACAi-001
CAWT + 1×Eb
CAWT + 2×Eb
(Denaturing condition)
MeOH
ACAi-001
Eb
29+
28+
Mr 25601.57
Mr 25600.72
25936.34
26270.47
26150.49
25950.27
Mr 25599.87
(m/z)
(Mass)
B
(0 h)
(72 h)
Tetramer (Tet)
Trimer (Tri)
Dimer (Dim)
Monomer (Mo)
Tet
Tri
Dim
Mo
Multimerization products
Degradation
DMSO
ACAi-001
RAL
PF74
ACAi-028
C
(0 h)
(72 h)
CAWT
DMSO
ACAi-001
Multimerization products
Degradation products
OD280
(ml)
D
DMSO
2
20
200 μM
ACAi-001
RAL
OD350
(min)
E
(0 h)
(72 h)
DMSO
2
20
200
ACAi-001
RAL
Tm 50
Relative fluorescence
Temperature (℃)
ΔTm 50
RAL
0.6
-0.6
-1.9
-8.7
-12.4
DMSO
2
20
200 μM
ACAi-001

Fig. 3

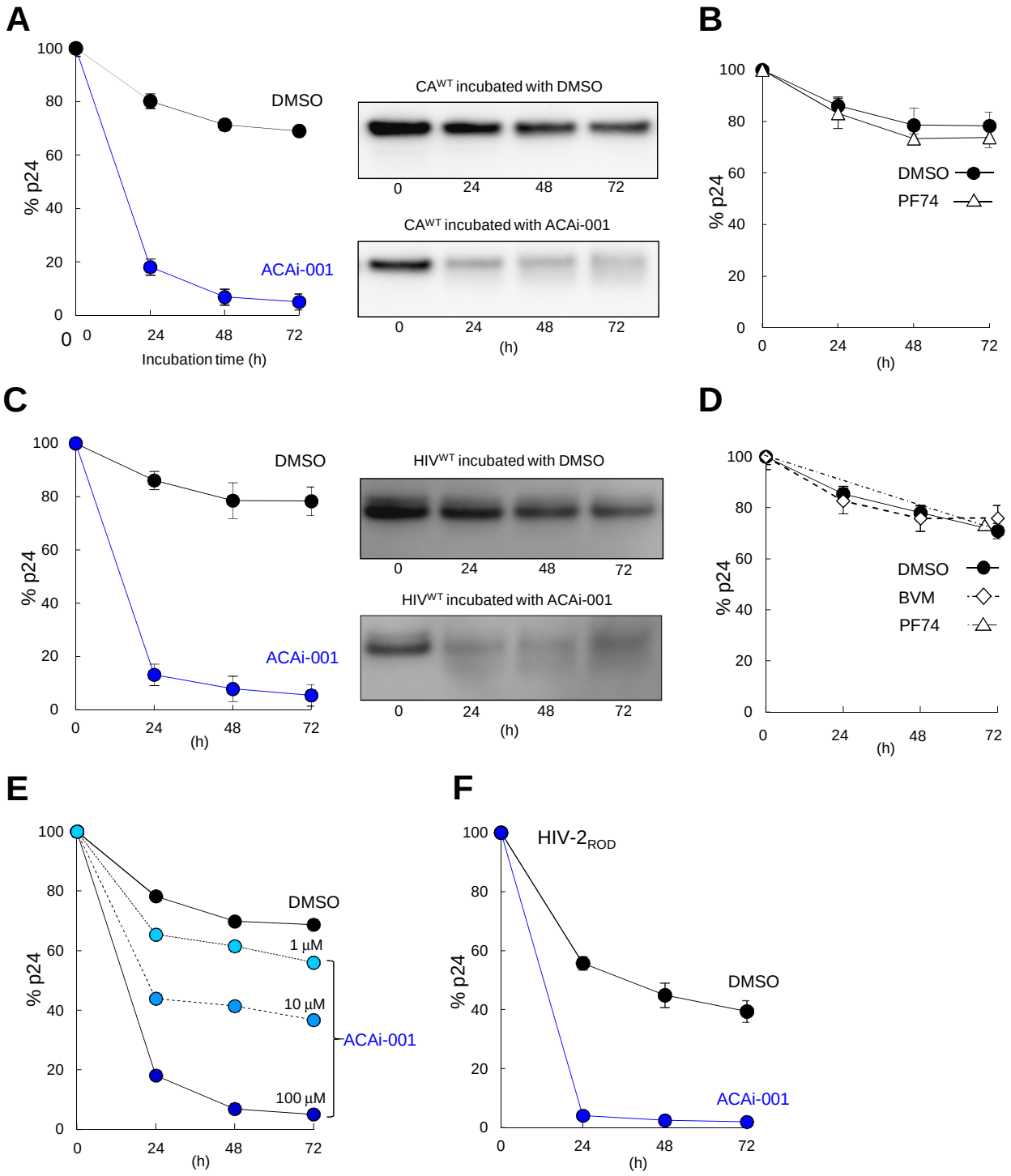
A
% p24
DMSO
ACAi-001
Incubation time (h)
CA^WT incubated with DMSO
CA^WT incubated with ACAi-001
(h)
B
DMSO
PF74
(h)
C
HIV^WT incubated with DMSO
HIV^WT incubated with ACAi-001
(h)
D
DMSO
BVM
PF74
(h)
E
DMSO
1 µM
10 µM
100 µM
ACAi-001
(h)
F
HIV-2ROD
DMSO
ACAi-001
(h)

Fig. 4

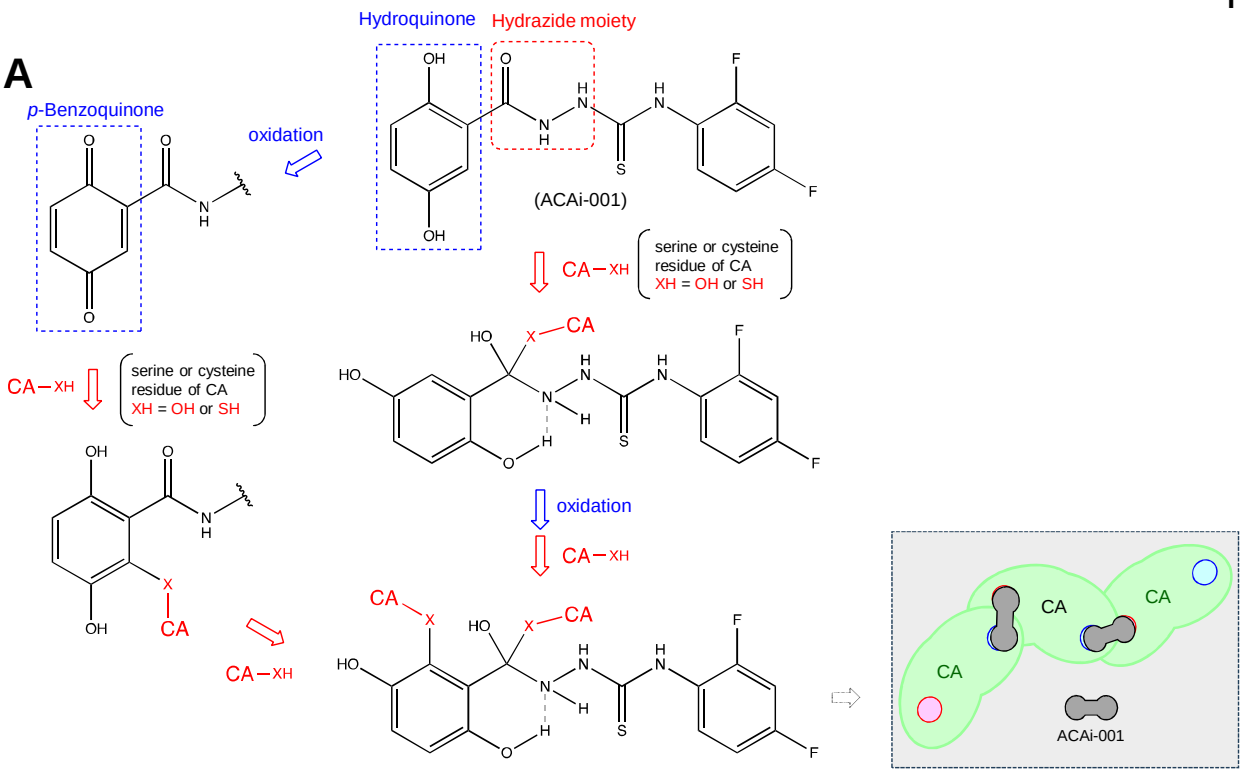
A
p-Benzoquinone
oxidation
Hydroquinone
Hydrazide moiety
(ACAi-001)
CA−XH
serine or cysteine residue of CA
XH = OH or SH
CA−XH
serine or cysteine residue of CA
XH = OH or SH
oxidation
CA−XH
CA−XH
CA
ACAi-001

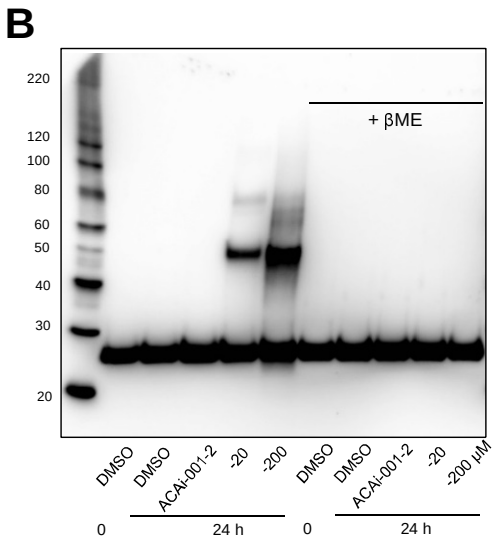
B
220
120
100
80
60
50
40
30
20
+ βME
DMSO
DMSO
ACAi-001-2
-20
-200
DMSO
DMSO
ACAi-001-2
-20
-200 μM
0
24 h
0
24 h

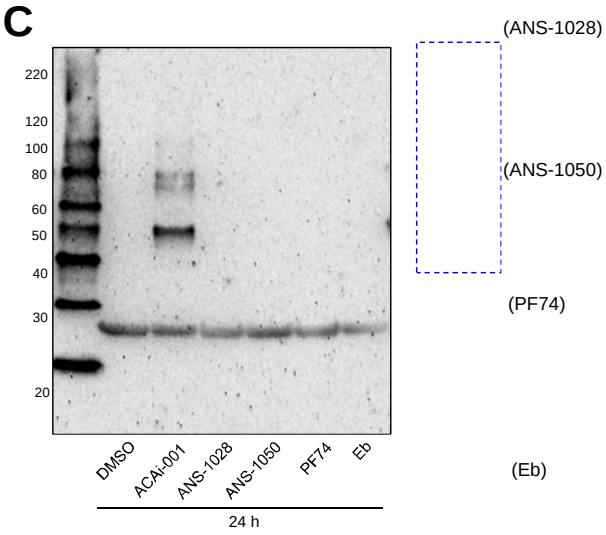
C
220
120
100
80
60
50
40
30
20
DMSO
ACAi-001
ANS-1028
ANS-1050
PF74
Eb
24 h
(ANS-1028)
(ANS-1050)
(PF74)
(Eb)

Fig. 5

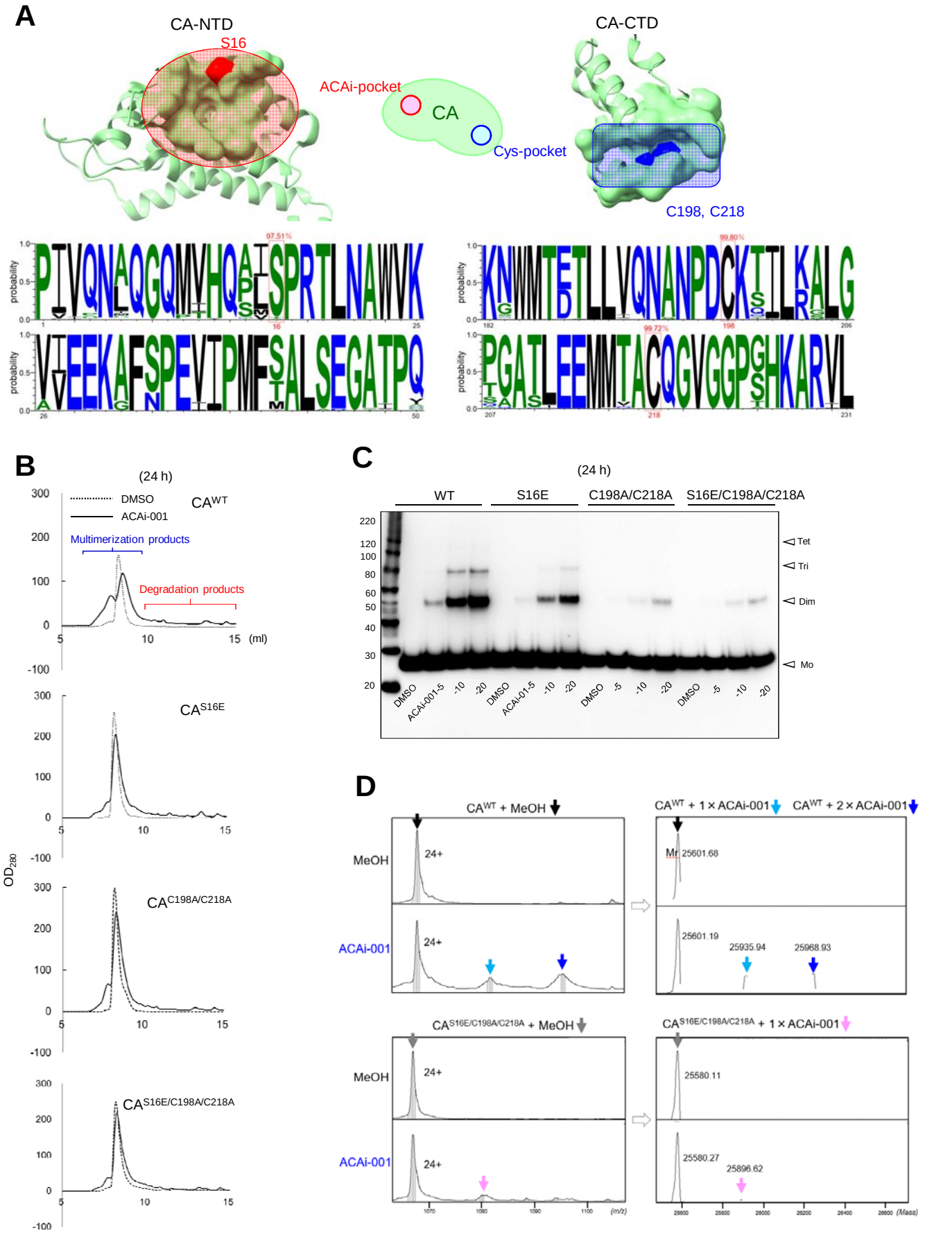
A
CA-NTD
S16
ACAi-pocket
CA
Cys-pocket
CA-CTD
C198, C218
probability
B
(24 h)
DMSO
ACAi-001
CA^WT
Multimerization products
Degradation products
(ml)
CA^S16E
CA^C198A/C218A
CA^S16E/C198A/C218A
OD280
C
(24 h)
WT
S16E
C198A/C218A
S16E/C198A/C218A
Tet
Tri
Dim
Mo
DMSO
ACAi-001-5
-10
-20
-5
D
CA^WT + MeOH
CA^WT + 1 × ACAi-001
CA^WT + 2 × ACAi-001
MeOH
ACAi-001
24+
Mr 25601.68
25601.19
25935.94
25968.93
CA^S16E/C198A/C218A + MeOH
CA^S16E/C198A/C218A + 1 × ACAi-001
25580.11
25580.27
25896.62
(m/z)
(Mass)

Fig. 6

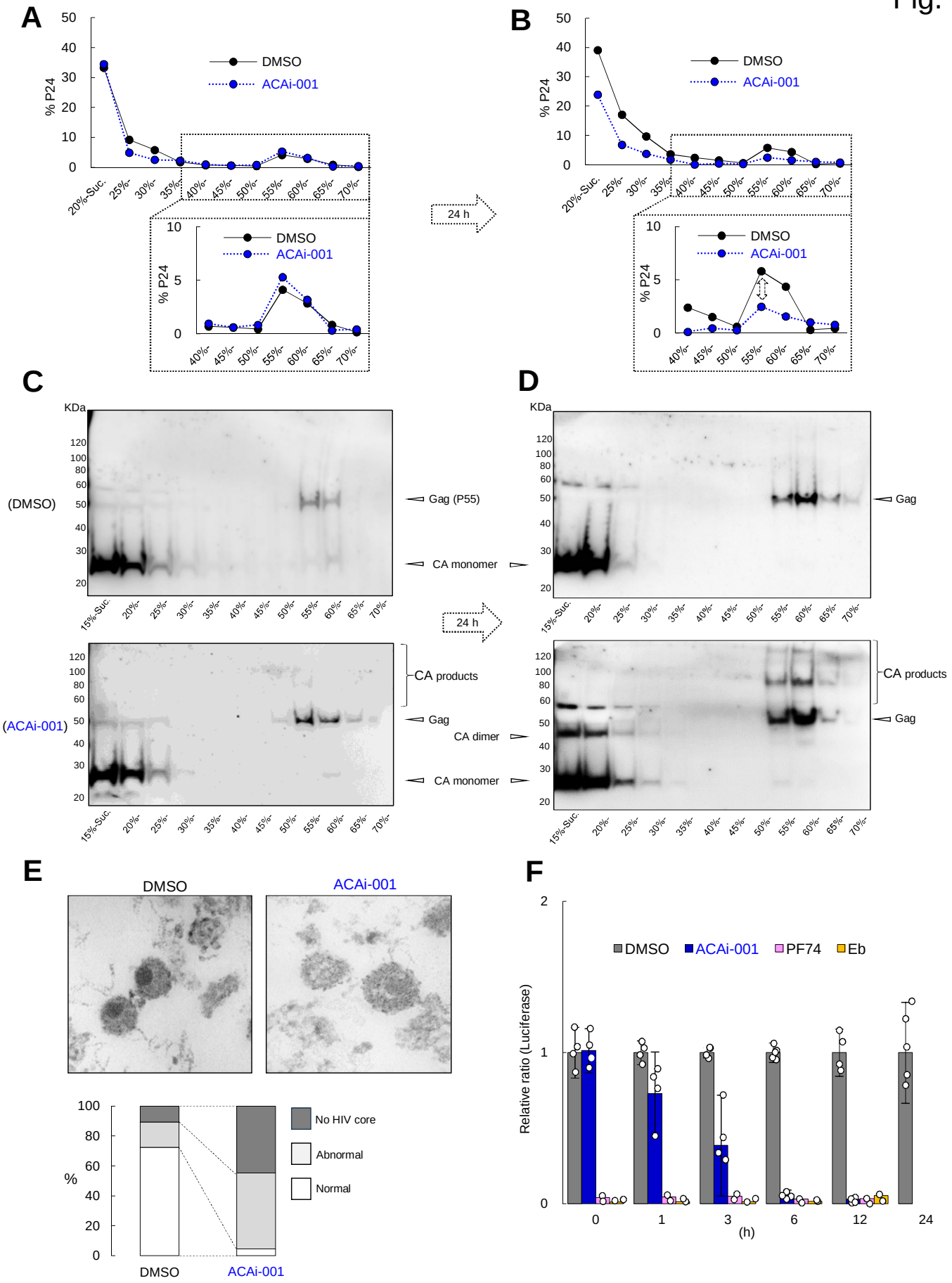
A
B
% P24
DMSO
ACAi-001
20%-Suc.
25%-
30%-
35%-
40%-
45%-
50%-
55%-
60%-
65%-
70%-
24 h
C
D
KDa
(DMSO)
(ACAi-001)
15%-Suc.
Gag (P55)
Gag
CA monomer
CA products
CA dimer
E
DMSO
ACAi-001
No HIV core
Abnormal
Normal
%
F
PF74
Eb
Relative ratio (Luciferase)
(h)